Preprints, 10th IFAC International Symposium on
Advances in Automotive Control
Columbus, Ohio, USA, August 28-30, 2022

Verification and improvement of flexible mathematical procedures for co-optimizing design and control of fuel cell hybrid vehicles

Manrique-Escobar C.A., Baldi C., Carmone S., Sorrentino M.

Department of Industrial Engineering, University of Salerno, Fisciano (Salerno), 84084-Italy

(Tel: 0039-089-96-4100; e-mail: cmanriqueescobar@unisa.it).

Abstract: A study on the usefulness of flexible mathematical tools for determining the optimal architecture of fuel cell hybrid vehicles is presented. Starting from a pre-existing powertrain and control strategies co-optimization tool, the technological (especially in terms of lithium battery type) search domain was first expanded by including an updated battery model. Afterward, the availability of specification independent control strategies was exploited in such a way as to enable two optimization tasks: one relying on previous heuristic control rules and the other based on newly optimized control strategies. The results evidenced negligible differences, in terms of key control variable trends, objective (i.e., fuel economy), and design parameters (i.e., fuel cell system size and battery energy density), thus further proving the tool versatility. Moreover, optimal configurations exhibit appreciable fuel economies and acceleration performance on the WLTP driving cycle, while proposing potentially cost-effective solutions in terms of fuel cell system size.

Keywords: PEM Fuel cell, Hybrid vehicles, Energy management, Specification independency, Control, Co-optimization

1. INTRODUCTION

Since the impact of climate change is deeply modifying the delicate equilibrium of the ecosystem, reducing the carbon footprint of all sectors involved is nowadays necessary and urgent. The ambitious yet incontrovertible perspective subscribed to during the Paris Agreement is a drastic reduction of pollutant emissions within 2030 (*Paris Agreement*, n.d.). The benefits of greener vehicles are undeniable: electric vehicles (EVs), hybrid electric vehicles (HEVs), and fuel cell hybrid vehicles (FCHVs) seem to be the best solution to re-establish acceptable levels of CO2, representing a valid performance alternative to the traditional ones. From this perspective, EVs and FCHEVs are attractive because they do not operate on a combustion basis. Furthermore, FCHVs may feature a more extensive autonomy range than the EVs, thanks to the higher energy density of hydrogen storage systems compared to the one of battery packs. However, the CO2 generation linked to the production of electricity and hydrogen respectively remains. In particular, since electricity and hydrogen production are not frequently green. Thus, the emissions are delocalized from the user location to the production one (Palmer et al., 2021). Besides, emissions linked to the components' production and disposal must also be accounted for (Hao et al., 2017).

In the perspective of a conscious usage of vehicles powered by hydrogen, a prudent sizing of the battery pack may lead to the development of FCHVs capable of effectively substituting the conventional ones. There are some contrasting examples of vehicles exhibiting different degrees of hybridization in the reference literature. Some of them tend to the unitary value, thus converging towards more range extender solutions, while others favor a lower power portion supplied by the battery, thus being more representative of full hybrid architectures (The New Toyota Mirai, n.d.). The tool developed in (Sorrentino et al., 2019) determines the proper configuration referring to the above solutions while pursuing a quasi-battery charge sustaining strategy. Such a goal must be achieved without any sacrifice in terms of acceleration performance guaranteed. This paper aims to refine the aforementioned pre-existing co-optimization mathematical tool for proton exchange membrane-based FCHVs, considering the employment of a new battery model, which better spans the current energy vs. power density sizing domain of lithium battery technology. The approach presented in this work results timely since, in general, the hybrid powertrain optimization methods proposed in the literature consider just a single type of cell (Jokela et al., 2019), (Sorrentino et al., 2019), or a small dataset of battery cell types (Zhou et al., 2022); thus, limiting the optimization design space.

The present work addresses the previously described limitation by exploring the energy density domain of the cell technology of interest through the well-known Ragone plot relation between energy density and power density of a battery cell technology. Consequently, it makes it possible to identify what type of cell is most convenient for a particular application at a more specific level. The goal is to upgrade the mentioned co-optimization procedure to extend the effective search domain, in which the optimal solution, in terms of powertrain sizing and energy management strategy (EMS) parametrization definition, can be achieved. The rule-based nature of the parameterized EMS is justified by its suitability to derive specification-independent control strategies and to facilitate the setting-up of design and energy management co-optimization tasks (Iqbal et al., 2021), being these features incompatible with traditional approaches such as Dynamic Programming or Pontryagin Minimum Principle (Onori et al., 2016). Therefore, another objective of the current study was to

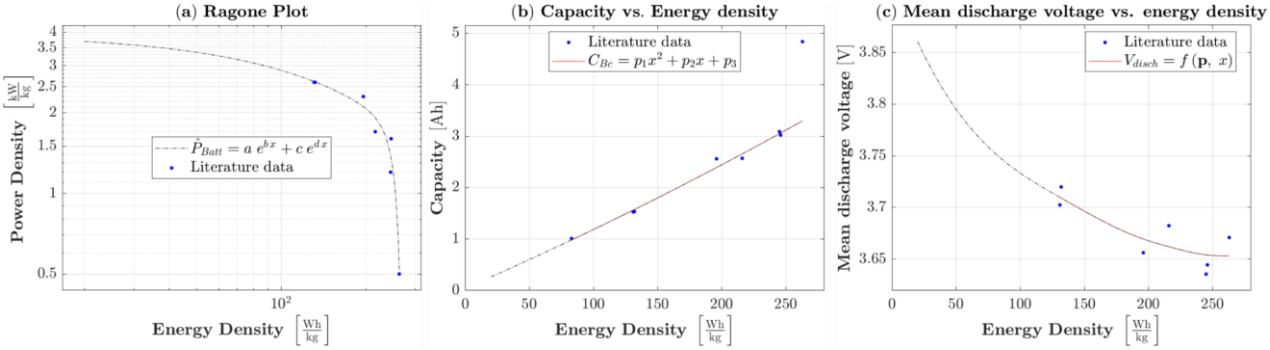

Figure 1. Mathematical model to estimate battery cell properties as function of the battery energy density. (a) Lithium-ion batteries Ragone plot. (b) Battery cell capacity estimation. (c) Battery cell mean discharge voltage estimation.

derive further control rules that strictly depend on the newly introduced parameterized battery-pack model mentioned. The final target was to apply the updated co-optimization procedure to representative driving cycles, test the adopted control strategies specification independence further, and prove the suitability of the proposed tool to identify the optimal FCHV configuration by exploring a larger technology search domain. The article is structured as follows: first, the updated battery cell's properties model is introduced, then the parametric dimensioning model utilized to define the mass impact on the vehicle design is presented. Afterward, the key concepts and formulas related to the specification independency of the adopted heuristic rules are recalled. Finally, the robustness of the design strategy is demonstrated via a comparison between the results of the original version of the tool and its revisited counterpart, updating the control rules as a function of the newly adopted battery model.

2. DESIGN AND CONTROL METHODOLOGIES

This section focuses on the design strategy adopted to simultaneously address the powertrain components sizing and the heuristically derived specification independent control strategy. The tool presented in this work, shown in Figure 2, enhances the one introduced in (Sorrentino et al., 2019). In particular, such a tool is integrated here with an algorithm parametrically defining the properties of battery cells to explore high-energy and high-power density lithium-ion battery design solutions. The remaining of this section presents the battery cells sizing algorithm, the FCHV's powertrain parametric dimensioning model, the battery pack model to simulate its performance during the simulation task, and the derivation of the optimized rule-based energy management of the hybrid powertrain during the driving phase.

2.1 Battery Cells Dimensioning

The optimal hybrid powertrain design is linked to the correct sizing of the fuel cell system (FCS) and battery pack. In particular, the latter's dimensioning is primarily defined by selecting high-power density or high-energy density battery cells. Such design criteria can be systematized by expressing the properties of battery cells as a function of the energy density, $\hat{E}_{Batt}$ [Wh/kg]. This approach is based on the univocal relationship between energy storage technologies' energy and power densities expressed via the so-called Ragone plot (Catenaro et al., 2021), which allows building a functional

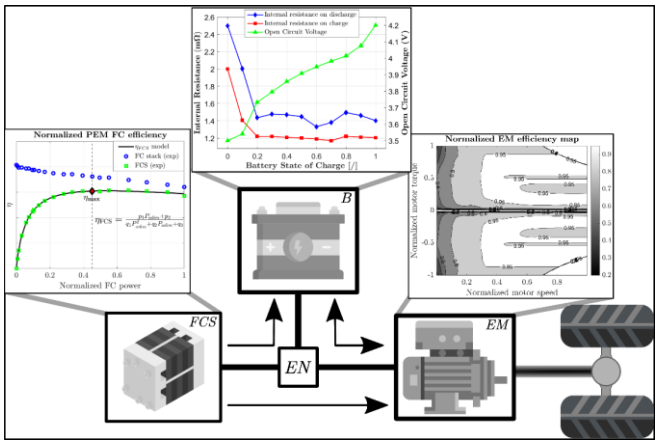

Figure 2. The hybrid powertrain model consists of a hydrogen fuel cell (FCS) and a battery pack (B), which feed in parallel an electric motor (EM) connected to the wheels of the vehicle. The efficiency of the FCS and EM are evaluated by means of the maps

relationship. The regression models shown in Figure are built with experimental data of multiple battery cells over a wide range of energy densities retrieved from (Lain et al., 2019). With these, it is possible to estimate the power density $\hat{P}_{Batt}$ [kW/kg], charge capacity C_{Bc} [Ah], and discharge voltage (V_{disch} [V]) of a battery cell as a function of its energy density. Then, the mass of a battery cell m_{Bc} [kg], its nominal power P^*_{Bc} [kW], and its energy content (Cap_{Bc} [Wh]) can be computed as follows:

$$Cap_{Bc} = C_{Bc} \cdot V_{disch}\ [\mathrm{Wh}] \tag{1}$$

$$m_{Bc} = \frac{Cap_{Bc}}{\hat{E}_{Batt}}\ [\mathrm{kg}] \tag{2}$$

$$P^*_{Bc} = \hat{P}_{Batt} \cdot m_{Bc}\ [\mathrm{kW}] \tag{3}$$

Once these properties are available for the battery cells, dimensioning the battery pack becomes straightforward. The designer can make decisions based on battery pack energy content (Cap_{Batt} [kWh]) or the nominal power of the required battery pack (P^*_{Batt} [kW]).

2.2 Powertrain Parametric Dimensioning

This section describes the approach for the powertrain systematic design of an FCHV. It starts from the properties of previously estimated battery cells and a given nominal power

of the FCS (P^*_{FCS} [kW]). Then, considering a weight/power ratio (ρ_{p2w} [kW/kg]), and the mass of the base chassis (M_{body} [kg]) of the vehicle class of interest, a set of algebraic expressions is formulated as follows:

$$\begin{cases} \rho_{p2w} = \dfrac{P^*_{EM}}{M_{FCHV}} = \dfrac{P^*_{ICE,CV}}{M_{CV}} \\ N_{Bc}\, P^*_{Bc} + P^*_{FCS} = P^*_{EM} \\ M_{FCHV} = M_{body} + M_{TH_2} + P^*_{EM}\, \hat{m}_{EM} + P^*_{FCS}\, \hat{m}_{FCS} + m_{Bc}\, N_{Bc} \end{cases} \tag{4}$$

where M_{CV} and $P^*_{ICE,CV}$ are the conventional vehicle (CV) mass and engine power; M_{TH_2} is the hydrogen's tank mass; $\hat{m}_{EM}$ and $\hat{m}_{FCS}$ are the mass per unit power in [kg/kW] of the EM and FCS respectively. The first expression in (4) imposes the ρ_{p2w} of a conventional of the FCHV to equal that of a CV. Besides, the number of the battery cells (N_{Bc}) is computed by equating the nominal power of the battery pack together with that of the FCS to the nominal power of the electric motor (P^*_{EM} [kW]). Finally, the total mass of the FCHV (M_{FCHV} [kg]) is computed by adding the contribution of all the hybridizing components.

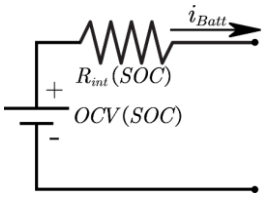

Figure 3. The equivalent circuit battery model to monitor the state of charge during operation.

2.3 Battery Model

To evaluate the state of charge (*SOC*) of the battery pack during its operation, in the present work an R-int type battery model (Mousavi G. & Nikdel, 2014) is used as shown in Figure . The open circuit voltage (OCV [V]) and the internal resistance of the battery pack (R_{int} [Ω]) during charge and discharge load are estimated as a function of the battery state of charge (SOC) by considering the experimental data from (Saxena et al., 2015) measured from a battery pack found in the literature (Saxena et al., 2015) and shown in Figure 2. Besides, the instantaneous SOC is evaluated via Coulomb counting approach by the following expression

$$SOC = -\frac{1}{3600 \cdot N_{Bc} \cdot C_{Bc}} \int i_{Batt}(t)dt + SOC_0 \tag{5}$$

where SOC_0 is the initial condition of the variable, and i_{Batt} [A] is the battery current computed as a function of the instantaneous power delivered (P_{Batt}) as follows

$$i_{Batt} = \frac{OCV(SOC) - \sqrt{(OCV(SOC))^2 - 4R_{\text{int}}(SOC)P_{Batt}}}{2R_{\text{int}}} \tag{6}$$

therefore, allowing to compute the SOC along the simulation.

2.4 Optimized Rule-based Energy Management Strategy

The EMS handles the control of the two power sources, namely the battery pack and the FCS, onboard the vehicle during the driving cycle. In this work, a rule-based EMS with optimized parameters developed in previous contributions

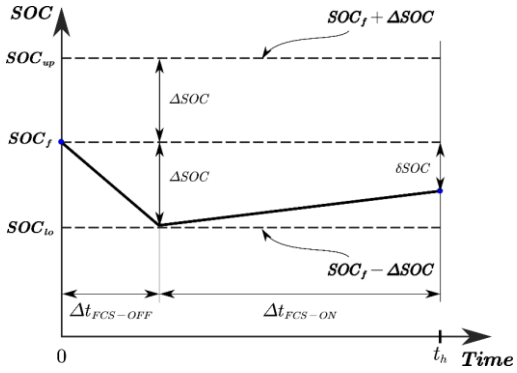

Figure 4. Optimization framework to construct the functions *f* and *g* for the optimal rule-based strategy.

(Sorrentino et al., 2011) is considered for testing its adaptability to the new battery pack sizing approach introduced in Section 2.1. The present algorithm parameterizes the power delivered by the FCS and allowed discharge level of the battery pack as function of the average power demanded by the drivetrain ($\bar{P}_{tr}$). The latter is calculated from a standardized driving cycle and the vehicle's longitudinal equation of motion. In this way, the instantaneous power of the FCS, P_{FCS} , and the discharge level, ΔSOC , of the battery pack with respect to a target level, SOC_f , can be expressed as:

$$P_{FCS} = f\left(\bar{P}_{tr}\right) \tag{7}$$

$$\Delta SOC = g\left(\bar{P}_{tr}\right) \tag{8}$$

where the functions f and g , to be referred to as control-maps, are constructed by considering the optimization framework presented in Figure . The scenario shown features a fixed time-horizon (t_h) in which a constant $\bar{P}_{tr}$ is supplied by the power sources during two different phases. First, a charge depleting phase in which only the battery pack supplies power, thus SOC varies from SOC_f to $SOC_f - \Delta SOC$. Then, during the second phase, the FCS operates exclusively with constant power P_{FCS} . The two parameters defining the control policy, namely P_{FCS} and ΔSOC are determined, for multiple values of $\bar{P}_{tr}$, by a nonlinear numerical optimization problem minimizing the following cost function

$$\min_{P_{FCS},\Delta SOC} \int_0^{t_h} \dot{m}_{\text{H}_2}\left(P_{FCS}, \Delta SOC\right)dt + \| \delta SOC \|$$
$$\text{s.t.} \tag{9}$$
$$P_{FCS} \in \left[0, P^*_{FCS}\right]$$

where the time integral of hydrogen mass flow during the time horizon is minimized as well as the term δSOC , which, as shown in Figure , is defined as

$$\delta SOC = SOC_f - SOC_{end} \tag{10}$$

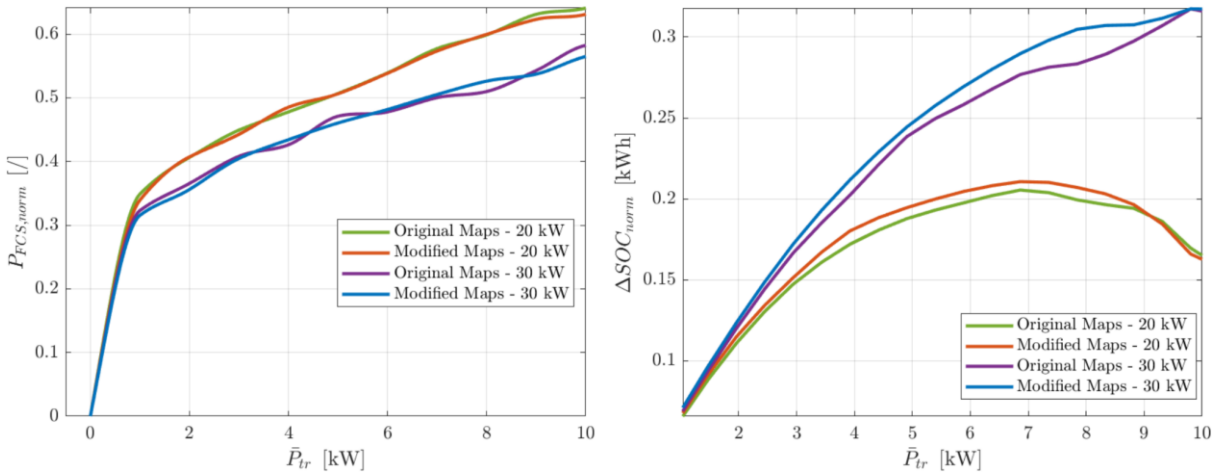

Figure 5. Normalized control maps of the control strategy for an extended range of mean traction power.

with SOC_{end} being the value at the end of the time horizon considered. The optimization framework previously described takes place by considering a reference powertrain featuring dimensioned components. Therefore, the computed control maps in (7) and (8) are characterized by the reference values $P^*_{FCS,ref}$ and $Cap_{Batt,ref}$ used to compute them. Thus, to promote the feasibility of the control algorithm at various powertrain sizing, the following expressions are formulated to normalize the optimization results:

$$P_{FCS,\text{norm}} = \frac{P_{FCS}}{P^*_{FCS,ref}} \qquad \Delta SOC_{norm} = \Delta\text{SOC} \cdot Cap_{Batt,ref} \tag{11}$$

Then, the control policy can be deployed for a different powertrain by denormalizing the control maps as follows

$$P_{tr,\text{denorm}} = \frac{\bar{P}_{tr}}{P^*_{FCS,ref}} P^*_{FCS} \qquad P_{FCS,\text{denorm}} = P_{FCS,norm} P^*_{FCS} \qquad \Delta SOC_{\text{denorm}} = \frac{\Delta SOC Cap_{\text{Batt},ref}}{Cap_{\text{Batt}}} \tag{12}$$

in this way generalizing the control maps for a wide range of hybrid powertrain designs. The above-recalled energy management strategy was proven effective via comparison with both genetic algorithm (Sorrentino et al., 2010) and dynamic-programming (Sorrentino et al., 2011) offline optimization tasks.

3. RESULTS

The normalized control maps of the energy management strategy, obtained through the previously described optimization framework, are presented in Figure . Two nominal power values for the reference powertrain's fuel cell system, $P^*_{FCS,ref}$, have been considered during the construction of the control maps, namely 20 and 30 [kW]. Besides, two different battery packs for each of these reference powers are employed, yielding two variants of the control maps, namely the *Original Maps* and the *Modified Maps*. The *Original Maps* are built using a battery pack with high-power density cells, sized following the procedure described in (Sorrentino et al., 2019). On the other hand, the *Modified Maps* consider a battery pack sized using the approach described in Section 2.1, which contemplates high-energy and high-power density batteries. The contrast between the *Original Maps* and *Modified Maps* curves in Figure demonstrates their robustness to the powertrain design considered during the offline optimization.

Table 1. The powertrain co-optimization strategy results, considering both the modified and original maps for 20 and 30 kW of FCS reference power. The table presents the optimal powertrain design parameters for each of the latter.

	$P_{FCS,ref}$ [kW]	20	30
Modified Maps	FE [km/kg]	114.2942	114.5162
	P^*_{FCS} [kW]	22.2635	21.2079
	$\hat{E}_{Batt}$ [Wh/kg]	76.9854	73.3321
	Battery capacity [kWh]	1.3666	1.3073
	P^*_{Batt} [kW]	54.85	55.67
Original Maps	FE [km/kg]	114.3141	114.4321
	P^*_{FCS} [kW]	22.1298	21.2471
	$\hat{E}_{Batt}$ [Wh/kg]	77.8213	71.7457
	Battery capacity [kWh]	1.3879	1.2705
	P^*_{Batt} [kW]	54.96	55.64

Furthermore, through the powertrain parametric dimensioning approach, introduced in Section 2.2, which allows sizing an FCHV powertrain having as inputs P^*_{FCS} and $\hat{E}_{Batt}$, a co-optimization procedure of the powertrain design was considered, homologous to the one presented in (Sorrentino et al., 2019). This approach takes the fuel economy (FE), defined as the ratio between the total traveled distance and the fuel consumed, as the objective function to maximize during a given driving cycle. Besides, the powertrain parametric dimensioning approach inputs are set as the design variables inside the numerical optimization routine as follows

$$\min_{P^*_{FCS},\hat{E}_{Batt}} \quad \frac{L}{m_{H_2}} \left[\frac{\text{km}}{\text{kg}}\right] \qquad \text{s.t.} \rightarrow t_{\text{PD-charge}} < 100 \ [s] \tag{13}$$

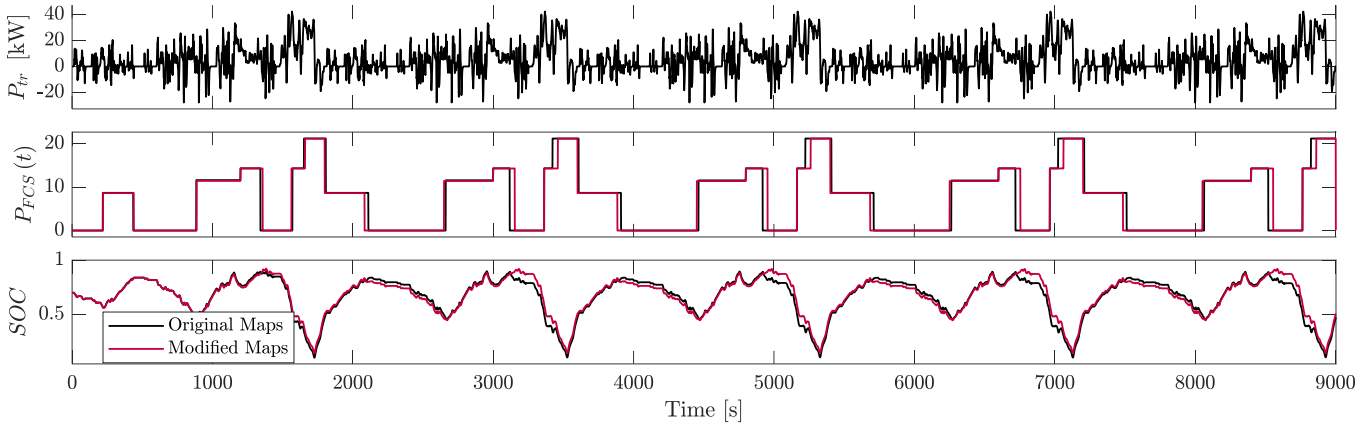

Figure 6: Comparison of the SOC and $P_{FCS}(t)$ during the complete driving cycle simulation power demand P_{tr}, using the original and modified maps variants

where L represents the total distance covered during the driving simulation; m_{H_2} is the total hydrogen mass consumed during the driving and posdriving recharge phase to restore its initial condition when required; and $t_{\text{PD-charge}}$ is the duration of such posdriving recharge. In the present work, a concatenation of five WLTP cycles is selected to approximate the full-day travel of a standard vehicle in a typical city (Tutuianu et al., 2015). Such a driving schedule is also suitable to test effective power-split deployability by performing model-based analyses featuring low-level controllers of PEM-based FCHV powertrains (Arsie et al., 2007). The results of this process are presented in Table 1. In general, the FCS nominal power, the battery energy density, battery pack capacity, and the optimal fuel efficiency for each of the cases considered vary slightly between the *Modified Maps* and *Original Maps* variants. For instance, the difference in the optimal fuel economy obtained for both variants, considering the 20 and 30 kW maps, varies by 0.017% and 0.073%, respectively. This fact confirms the robustness of the control algorithm to the powertrain design parameters. In addition, it is worth highlighting that the maximum fuel economy value reported in Table 1 is comparable to the value reported in (*The New Toyota Mirai*, n.d.). This shows that the proposed mathematical tool allows identifying the optimal powertrain design, presenting a low FCS nominal power and, therefore, cost containment in future FCHV deployment scenarios, which meet major automakers' performance and consumption requirements.

Finally, the dynamics of the SOC and the power delivered by the FCS during the driving cycle simulation are considered to further evaluate the difference on the energy management strategy for the Original Maps and the Modified Maps variants. The powertrain design considered is that yielding the higher fuel economy from Table 1, that is:

$$\begin{aligned} P_{FCS}^{*} &= 21.2079\,[\text{kW}] \\ \hat{E}_{Batt} &= 73.3321\,[\text{Wh/kg}] \end{aligned} \tag{14}$$

Figure present the behavior of the SOC dynamics and the control policy of the FCS power for both variants during the simulation of the driving cycle. In general, from Figure , the behavior of the *SOC* follows the same trend for both control maps variants. The difference between both curves lies mainly in the depth of discharge, being slightly more prominent for the *Modified Maps* variant. A similar observation emerges from Figure 6., where both control policies follow the same pattern, except for minor differences in the time of occurrence of some steps and their magnitude. In order to obtain a quantitative measure of the similarity of these variables, it is calculated the root mean squared error (RMSE) of the signals as follows

$$RMSE = \sqrt{\frac{1}{m}\sum_{m}\left(SOC_{MM}(t) - SOC_{OM}(t)\right)^2} \tag{15}$$

where m is the number of data samples of both signals, SOC_{MM} is the SOC time signal of the *Modified Maps* variant, and SOC_{OM} the SOC time signal of the *Original Maps* variant. This index is equal to 0.0384 for the SOC time signal, and, analogously, for the $P_{FCS}(t)$ yields 2.6396. Both numeric indicators of high similarity between the simulation results featuring the two control maps variants.

4. CONCLUSIONS

This work presents a mathematical tool for the parametric dimensioning of an FCHV, its specification independent energy management strategy formulation, and the co-optimization of both design and energy management strategy by considering the fuel economy as the objective function. In particular, the present work is a continuation of the results presented in a previous authors contribution. The contribution herein consists of proposing an improved algorithm for the sizing of the FCHV battery pack that considers battery cells with high-energy density and high-power density through the univocal relationship between these properties through the so-called Ragone plot. Additionally, the verification of the robustness of the control algorithm proposed for the energy management strategy is demonstrated by varying the parametric dimensioning model of the FCHV and the driving cycle employed during the co-optimization. In particular, the present work considers a concatenation of five WLTP cycles, resulting in a highly demanding driving test.

The robustness of the present tool has been analyzed qualitative and quantitatively via the analysis of the resulting normalized control maps, the co-optimization results analysis, and the driving cycle simulation of both the *Original Maps* and

the *Modified Maps* variants. The negligible percentage differences in the optimal fuel economy and the RMSE between the *SOC* dynamics and the FCS power supply of both variants confirm the tool's robustness.

Therefore, with the new battery model, the extension to more critical/demanding cycles such as WLTP and the confirmation of the versatility and specification independence of the control maps are proven. Consequently, the present mathematical tool lends itself to an extended analysis to perform optimal design choices, while taking into account multiple variables and exogenous factors. In this way, by defining appropriate objective functions and constraints, it will be possible to create a tool that identifies the best design solution depending on the boundary conditions. These will include the cost of components, availability of hydrogen, refueling station, recharging stations, plugin, or charge sustaining configuration, to name a few.

REFERENCES

Arsie, I., Di Domenico, A., Pianese, C., Sorrentino, M. (2007). Modeling and analysis of transient behavior of polymer electrolyte membrane fuel cell hybrid vehicles. Journal of Fuel Cell Science and Technology, 4:261–71.

Catenaro, E., Rizzo, D. M., & Onori, S. (2021). Experimental analysis and analytical modeling of Enhanced-Ragone plot. *Applied Energy*, *291*, 116473.

Hao, H., Mu, Z., Jiang, S., Liu, Z., & Zhao, F. (2017). GHG Emissions from the Production of Lithium-Ion Batteries for Electric Vehicles in China. *Sustainability*, *9*(4), 504.

Jokela, T., Iraklis, A., Kim, B., & Gao, B. (2019). *Combined Sizing and EMS Optimization of Fuel-Cell Hybrid Powertrains for Commercial Vehicles*. 2019-01–0387.

Lain, Brandon, & Kendrick. (2019). Design Strategies for High Power vs. High Energy Lithium Ion Cells. *Batteries*, *5*(4), 64.

Mousavi G., S. M., & Nikdel, M. (2014). Various battery models for various simulation studies and applications. *Renewable and Sustainable Energy Reviews*, *32*, 477–485.

Onori, S., Serrao, L., & Rizzoni, G. (2016). *Hybrid Electric Vehicles*. Springer London.

Palmer, G., Roberts, A., Hoadley, A., Dargaville, R., & Honnery, D. (2021). Life-cycle greenhouse gas emissions and net energy assessment of large-scale hydrogen production *via* electrolysis and solar PV. *Energy & Environmental Science*, *14*(10), 5113–5131.

Paris Agreement. (n.d.). Retrieved March 7, 2022, from https://ec.europa.eu/clima/eu-action/international-action-climate-change/climate-negotiations/paris-agreement_en

Saxena, S., Le Floch, C., MacDonald, J., & Moura, S. (2015). Quantifying EV battery end-of-life through analysis of travel needs with vehicle powertrain models. *Journal of Power Sources*, *282*, 265–276.

Sorrentino, M., Cirillo, V., & Nappi, L. (2019). Development of flexible procedures for co-optimizing design and control of fuel cell hybrid vehicles. *Energy Conversion and Management*, *185*, 537–551.

Sorrentino, M., Pianese, C., & Maiorino, M. (2013). An integrated mathematical tool aimed at developing highly performing and cost-effective fuel cell hybrid vehicles. *Journal of Power Sources*, *221*, 308–317.

Sorrentino, M., Rizzo, G., & Arsie, I. (2011). Analysis of a rule-based control strategy for on-board energy management of series hybrid vehicles. *Control Engineering Practice*, *19*(12), 1433–1441.

The New Toyota Mirai. (n.d.). Toyota Europe Newsroom. Retrieved March 1, 2022, from https://newsroom.toyota.eu/the-new-toyota-mirai/#:~:text=Improvements%20in%20performance%20and%20efficiency&text=Despite%20the%20higher%20output%2C%20fuel,by%20the%20previous%20generation%20model.

Tutuianu, M., Bonnel, P., Ciuffo, B., Haniu, T., Ichikawa, N., Marotta, A., Pavlovic, J., & Steven, H. (2015). Development of the World-wide harmonized Light duty Test Cycle (WLTC) and a possible pathway for its introduction in the European legislation. *Transportation Research Part D: Transport and Environment*, *40*, 61–75.

Zhou, J., Feng, C., Su, Q., Jiang, S., Fan, Z., Ruan, J., Sun, S., & Hu, L. (2022). The Multi-Objective Optimization of Powertrain Design and Energy Management Strategy for Fuel Cell–Battery Electric Vehicle. *Sustainability*, *14*(10), 6320.